ANL/ET/CP-100288

Hydrodynamic Effects of Eroded Materials on Response of Plasma-Facing Component during a Tokamak Disruption*

Ahmed Hassanein
Isak Konkashbaev

Argonne National Laboratory, USA

Presented at the 9th International Conference on
Fusion Reactor Materials (ICFRM-9)
Oct. 10-15, 1999, **Colorado Springs, Co.**

---

*Work is supported by the U.S. Department of Energy, Office of Fusion Energy Sciences, under Contract W-31-109-Eng-38.

DISCLAIMER

DISCLAIMER

Portions of this document may be illegible in electronic image products. Images are produced from the best available original document.

Hydrodynamic Effects of Eroded Materials on Response of Plasma-Facing Component during a Tokamak Disruption

A. Hassanein and I. Konkashbaev*

Argonne National Laboratory, Argonne, IL 60439, USA

Abstract

Loss of plasma confinement causes surface and structural damage to plasma-facing materials (PFMs) and remains a major obstacle for tokamak reactors. The deposited plasma energy results in surface erosion and structural failure. The surface erosion consists of vaporization, spallation, and liquid splatter of metallic materials, while the structural damage includes large temperature increases in structural materials and at the interfaces between surface coatings and structural members. Comprehensive models (contained in the HEIGHTS computer simulation package) are being used self-consistently to evaluate material damage. Splashing mechanisms occur as a result of volume bubble boiling and liquid hydrodynamic instabilities and brittle destruction mechanisms of nonmelting materials. The effect of macroscopic erosion on total mass losses and lifetime is evaluated. The macroscopic erosion products may further protect PFMs from severe erosion (via the droplet-shielding effect) in a manner similar to that of the vapor shielding concept.

---

*Permanent address: Troitsk Institute for Innovation and Fusion Research, Russia.

1. Introduction

Interaction of powerful plasma and particle fluxes with plasma-facing materials (PFMs) due to loss of plasma confinement in a tokamak can cause significant damage to exposed surfaces and nearby components. Erosion and structural damage remain major obstacles to a successful tokamak reactor concept. The extent of such damage depends on the detailed physics of the disrupting plasma, the physics of plasma/material interactions, and the design configuration of the plasma-facing components (PFCs). Plasma instabilities such as hard disruptions, edge-localized modes (ELMs), and vertical displacement events (VDEs) can cause both surface and bulk damage to surface and structural materials [1]. Surface damage includes high erosion losses from surface vaporization, spallation, and melt-layer erosion. Bulk damage includes large temperature increases in structural materials and at the interfaces between surface coatings and the structure, resulting in high thermal stresses, possible melting, and material fatigue and failure. The transport and deposition of the eroded surface materials to nearby components are also of major concern for plasma contamination and for successful and prolonged plasma operation following instability events.

The comprehensive computer simulation package **H**igh **E**nergy **I**nteraction with General **H**eterogeneous **T**arget **S**ystems (**HEIGHTS**) has been developed and used to study in detail the various effects of sudden high-energy deposition of different sources on target materials [2]. The HEIGHTS package consists of several integrated models that follow the beginning of a plasma disruption at the scrape-off layer (SOL) to the transport of the eroded debris and splashed target materials that result from the deposited plasma energy. To evaluate the magnitude of various damage mechanisms caused by plasma instabilities, comprehensive 2-D radiation magnetohydrodynamic (MHD) models are implemented in the HEIGHTS package by using advanced numerical techniques such as Particle-in-Cell and Ray Tracing methods. Detailed physical models of plasma/solid-liquid/vapor interaction in a strong oblique magnetic field have also been developed, in a

fully self-consistent 2-D heat conduction with phase change and thermal hydraulic models that are coupled with radiation and vapor MHD models.

Our present work focuses mainly on modeling the behavior and macroscopic erosion of metallic surfaces with a liquid layer that is subject to various forces, as well as on explosive erosion and the characteristics of brittle-destruction erosion of carbon-based materials (CBMs). Total erosion damage to PFCs due to plasma instabilities should include surface vaporization loss, erosion damage to nearby components from intense vapor radiation and deposition, and macroscopic erosion from liquid-metal splashing and brittle destruction of CBMs. Lifetime estimates of PFMs due to disruption erosion in a tokamak device are presented. Other factors that influence the lifetime of target materials and nearby components, such as loss of vapor-cloud confinement and vapor removal due to MHD effects and damage to nearby surfaces due to intensive vapor radiation can be studied with the HEIGHTS package.

2. Erosion Mechanisms

The vapor cloud that quickly develops above the surface material during a disruption, if well confined, will shield the original surface from the incoming energy flux and significantly reduce the heat load onto the exposed plate surface [1,3]. This shielding layer completely absorbs the incoming particle flux and as a result, the vapor cloud is heated to temperatures of up to several tens of eV. At such temperatures, the vapor plasma radiation W_{rad} becomes comparable with the incoming power W_p. Because of absorption by a colder, denser, and correspondingly more optically thick vapor plasma near the exposed surface, radiation power to the plate surface is significantly decreased.

2.1 Surface vaporization

To calculate the shielding efficiency of vapor cloud in protecting PFMs, detailed physics of plasma/vapor interactions have been modeled. The models include plasma-particle slowdown and energy deposition in the expanding vapor, vapor heating,

excitation, and ionization, and vapor-generated photon radiation. The detailed vapor motion above the exposed surface is calculated by solving the vapor MHD equations for conservation of mass, momentum, and energy under the influence of a strong magnetic field [2]. A significant part of the incident plasma kinetic energy is quickly transformed into vapor-generated photon radiation. Therefore, multidimensional models for photon transport throughout the expanding vapor cloud have been developed to calculate the net heat flux that reaches the original disruption surface of PFCs, as well as the radiation heat load reaching various nearby components. This net heat flux reaching the surface will then determine the net erosion from surface vaporization and erosion from liquid splashing and brittle destruction of PFCs during these instabilities.

Figure 1 shows a typical time evolution of a tungsten-surface temperature, melt-layer thickness, and vaporization losses during a disruption for an incident plasma energy of 10 MJ/m^2 deposited in a disruption time of 1 ms, as predicted by the HEIGHTS package [2]. An initial magnetic field strength of 5 T with an incident angle of 2° is assumed in this analysis. The sharp initial rise in surface temperature is due to the direct energy deposition of incident plasma particles at the material surface. The subsequent decrease in surface temperature is caused by the shielding effect of the eroded material accumulated above the target surface. The subsequent target behavior is determined mainly by the energy flux from the emitted photon radiation in the vapor cloud. HEIGHTS calculations predict that radiation power W_s onto the target surface is <10% of the original incident power ($W_s < 0.1\ W_p$) because of the shielding effect [3]. As vapor accumulates above the surface, it becomes more opaque to photon radiation, and therefore less energy is transmitted to the target surface, in turn resulting in less splashing and vaporization.

2.2 Macroscopic liquid erosion and brittle destruction

Net radiation power reaching the target surface will result in surface vaporization and surface ablation, i.e., mass loss in the form of macroscopic particles. Modeling predictions have shown that surface vaporization losses of metallic materials are small (only a few micrometers deep; see Fig. 1) due to the self-shielding effect over a wide

range of plasma conditions during shorter plasma instabilities. However, for a liquid metal surface, ablation was predicted theoretically to be in the form of macroscopic metal droplets due to splashing of the molten layer [4]. Simulation experiments to predict erosion of candidate PFMs during a plasma disruption have also shown that erosion of metallic materials (such as W, Be, Al, and Cu) can be much higher than mass losses due only to surface vaporization. These mass losses depend strongly on experimental conditions such as level of incoming power, existence of a strong magnetic field, target inclination, etc. [5-7]. The mass losses are found to be in the form of liquid metal droplets with average sizes of a few tens of micrometers leaving the target surface with velocities $V \approx 10$ m/s. Such ablation occurs as a result of splashing of the liquid layer mainly due to boiling and explosion of gas bubbles in the liquid, absorption of plasma momentum, and hydrodynamic instabilities developed in the liquid layer from various forces [8].

Hydrodynamic instabilities (such as Kelvin-Helmholtz and Rayleigh-Taylor instabilities) can occur if the vapor plasma is not well confined by the magnetic field and vapor flow occurs along the target surface [9]. Volume bubble boiling [4,10] usually occurs from overheating of the liquid metal above the vaporization temperature at which saturation pressure is equal to the outer pressure of the vapor plasma above the exposed target surface. Therefore, splashing erosion energy is roughly equal to the sum of the thermal energy (required to heat the liquid above a certain temperature, i.e., melting temperature for hydrodynamic instabilities and vaporization temperature for bubble boiling), melting energy (i.e., heat of fusion), and kinetic energy of the droplets. The kinetic energy of the splashed droplets is determined from the surface tension of the liquid metal.

Nonmetallic materials such as graphite and CBMs have also shown large erosion losses significantly exceeding that from surface vaporization. This has been observed in various disruption simulation facilities such as electron beams [11], laser [12], and plasma guns [13]. This macroscopic erosion of CBMs depends on three main parameters: net power flux to the surface, exposure time, and threshold energy required for brittle

destruction. The required energy for brittle destruction is critical in determining the net erosion rate of CBMs; for a graphite similar to MPG-9 graphite, it is estimated to be ≈10 kJ/g, or 20 kJ/cm^3 [13]. As an example, assuming a net power flux to the material surface during the disruption of ≈300 kW/cm^2, the deposited energy for a time of 1 ms is ≈0.3 kJ/cm^2, which then results in net erosion of ≈150 μm per disruption. This value is significantly higher than that predicted from pure surface vaporization of ≈10 μm per disruption for CBMs [14]. Therefore, more-relevant experimental data and additional detailed modeling are needed to evaluate the erosion of CBMs, which strongly depends on the type of carbon material.

To correctly predict macroscopic erosion due to ablation, a four-moving-boundaries problem is solved in the HEIGHTS package. The front of the vapor cloud is one moving boundary determined by solving vapor hydrodynamic equations. The second moving boundary due to surface vaporization of the target is calculated from target thermodynamics. Immediately following the surface vaporization front is a third moving boundary due to the melt-splashing front. Finally, the fourth moving boundary is at the liquid/solid interface, which further determines the new thickness of the melt layer. These moving boundaries are interdependent, and a self-consistent solution must link them dynamically and simultaneously. The third moving boundary (the liquid splashing front) will, however, determine the extent of metallic PFC erosion and lifetime due to plasma instabilities. The SPLASH code, part of the HEIGHTS package, calculates mass losses by using a splashing-wave concept as a result of each erosion-causing mechanism [15]. Thus, total erosion is calculated from the sum of all possible erosion mechanisms.

3. Macroscopic or Droplet-Shielding Concept

The ejected macroscopic particles from CBMs or splashed droplets from liquid surfaces (both referred as MP) will also form a cloud near the target surface. Therefore, accurate calculations of mass losses require full description of the media near the target surface, which consist of a mixture of vapor and droplets/macroscopic particles moving away from the surface. Photon radiation power from the upper vapor regions will then be

absorbed by the target surface, as well as by the mixture of both vapor and droplets cloud above the surface. This will result in more surface vaporization of both target and droplet surfaces. Therefore, in such a mixture of erosion products, further screening of the original target surface occurs due to MP. This has the effect of reducing photon radiation power to the target surface. Such screening is called "droplet shielding" in an analogy to the vapor shielding effect [1]. Figure 2 is a schematic illustration of the droplet or macroscopic shielding concept during plasma/material interaction following loss of plasma confinement. Features of droplet shielding and its influence on total mass loss are given below for the cases of volume bubble boiling with homogeneous velocities of droplets in momentum space, and Rayleigh-Taylor instability with droplets that move normal to the surface preferentially.

Heating of the target surface is due mainly to photon radiation, heat conduction, and direct particle impingement from the SOL to the surface. During a quasistationary phase, vapor heat-conduction downstream, i.e., $W_k = k_v \nabla T$, is equilibrated by the heat flux upstream, i.e., $W_{conv} = c_v V_{vapor} T$, carried by the vapor flux away from the surface, where k_v is vapor heat conductivity, c_v is vapor specific heat, and V_{vapor} is vapor velocity upstream:

$$W_K = K_V \nabla T = W_{conv} = c_V T V_{vapor}. \qquad (1)$$

The net heat flux $W_{net} = W_k - W_{conv}$ toward the surface is very small. This is usually the case when radiation power to the surface exceeds a few hundred kW/cm^2 where intense vaporization takes place depending on target material properties (temperature and energy of vaporization). Therefore, the net heat flux from vapor cloud to target surface can be neglected in comparison with vapor cloud radiation.

Much of the radiation reaching the target surface is usually emitted by a narrow layer some distance from the target surface, with a vapor temperature approximately equal to the vapor-plasma ionization temperature, since photons with short wavelengths from hot regions are absorbed by the colder and more denser plasma. For candidate

materials such as W, C, Be, and Li, the luminance temperature is governed by T_{max} of a few eV, depending on the atomic number; therefore, radiation power to target surface is $\approx W_{rad} = \sigma T^4 \leq 1$ MW/cm^2.

At longer times, heat conduction into the target plate is proportional to $t^{-1/2}$ and can be neglected. Thus, most radiation coming to the target surface is spent in erosion, i.e., mass losses due to vaporization and ablation. Consideration of droplet shielding will further be provided by using an analytical solution to provide insight to the role of the various physical and material processes controlling overall erosion mechanisms during disruptions. The analytical solution is complementary to the detailed numerical models used to study vapor and droplet shielding phenomena and that are implemented in the HEIGHTS package.

The emitted MP usually have a distribution in both particle size and velocity. For the analytical solution, we consider only particles with an average radius R_d and velocity U in the normal direction to target surface. Heat conduction from the vapor to MP is very small and is neglected; thus MP are heated only by photon radiation. Because MP will absorb some of the photon radiation, only part of this radiation, W_s, achieves the plate surface, $W_s < W_o$, where W_o is the total photon radiation flux toward the target surface that is generated at greater distances from the surface where the hot vapor plasma exists. This part of the radiation reaching the surface is also spent in additional vaporization and ablation, i.e., MP formation. Because vaporization energy per gram q_v is much higher than the energy for ablation q_d, surface radiation power is mostly spent in MP formation. The number of MP per unit volume, i.e., density of MP n_{do}, with an average radius R_{d0} leaving the surface with a velocity V_{d0} is given by

$$n_{d0} = \frac{W_s}{q_d V_{d0} U}, \text{ where } V_{d0} = \frac{4}{3}\pi R_{d0}^3 , \tag{2}$$

$$q_d = q_{th} + \Delta q , \; q_{th} \approx c_v T_s , \text{and } \Delta q = q_n + q_k , \tag{3}$$

where q_d is destruction energy (for liquid splashing or brittle destruction), q_n is the energy required to separate MP from the surface, q_k is kinetic energy of MP, c_v is specific heat, and T_v is vaporization temperature, i.e., the saturation temperature at the corresponding vapor pressure above the target surface. Both q_k and q_n are calculated to be very small compared to q_{th} and will be ignored in the analytical solution.

Because ejected MP from target surface will absorb photon radiation, the equation for the spatial variation of the radiation power W is

$$\frac{dW}{dx} = -\frac{W}{l_v};\ l_v = \frac{1}{n_d \sigma};\ \sigma = \zeta \pi R_d^2, \tag{4}$$

where ζ is absorption coefficient, $\zeta \leq 1$, and l_v is mean path length of photons. The absorbed energy is mainly spent in the vaporization of MP:

$$U\frac{dV_d}{dx} = -\frac{W}{q_v}\sigma. \tag{5}$$

Equations 4 and 5 have a solution with the ratio between W_s and W_o given by

$$\frac{W_s}{W_o} = \frac{1}{1+\lambda}\ , \text{and } \lambda = \frac{q_v}{q_d} \tag{6}$$

Therefore, radiation power to the surface decreases by a factor $(1+\lambda)^{-1}$ due to droplet shielding. For a lithium target, q_d (T = 1290 K) $\approx$ 2.55 kJ/cm^3 and $q_v \approx$ 9.33 kJ/cm^3; thus $\lambda = q_v/q_s \approx 3.66$, and $W_s/W_0 = 0.2$, i.e., only $\approx$20% of the incoming radiation energy is deposited directly on the target surface.

It is interesting to note that W_s does not depend on other parameters such as MP initial radius R_{d0} or velocity U, which are not well defined. This means that the ratio W_s/W_0 does not depend on size or velocity distributions of the ejected MP, but only on energies of destruction q_d and vaporization q_v. Therefore, this prediction is valid for an arbitrary distribution of droplet velocities in momentum space.

The distance L at which MP are entirely vaporized, i.e., when $R_d = 0$, can then given by

$$\frac{L}{R_{do}} = U\frac{q_v}{W_o}\frac{4}{\zeta}F\,, \quad F = \frac{\nu_0}{u_0}\,, \tag{7}$$

$$\nu_0 = \tfrac{1}{3}\ln\frac{\sqrt{1+u_0+u_0^2}}{1-u_0} + \frac{1}{\sqrt{3}}\operatorname{arctg}\frac{u_0\sqrt{3}}{2+u_0}\,,$$

$$u_0 = \sqrt[3]{\frac{\lambda}{1+\lambda}}\,. \tag{8}$$

Usually, $10 > \lambda > 1$; thus $u_0 \approx 1$ and $1 < F < 20$. For example, for a liquid lithium target, $F(\lambda = 3.7) = 7.85$ and for $\zeta \approx 1$;

$$\frac{L}{R_{d0}} \approx 7.7\frac{U(m/s)}{W_0(MW/cm^2)}. \tag{9}$$

The average droplet size R_d and the average velocity U were measured only for an Al target in disruption simulation experiments [5,7]. According to the experimental results, droplet velocity is $U \approx 10$ m/s and R_{do} is a few tens of micrometers, $R_{do} \geq 10^{-3}$ cm. The radiation power to a divertor surface during a plasma disruption is calculated to be $W_0 \approx 0.8$ MW/cm^2 for a lithium target [1]. If the lithium droplets have similar size and velocity distribution as the Al droplets, they will be vaporized at a distance $L \approx 100\ R_{d0}$, i.e., $L < 1$ cm.

Carbon-based materials vaporize in the form of mon- and multiatomic molecules C_1, C_2, C_3, etc., depending on surface temperature. For a carbon divertor plate, the vaporization energy for sublimation is in the form of monatomic gas: $q_v(C_1) \approx 134$ kJ/cm^3 and $T_v \approx 4473$ K. Therefore, a minimum value of $q_d \approx 11.2$ kJ/ cm^3 yields $\lambda(C_1) \approx 10$ and $W_s/W_0 \approx 0.1$, i.e., <10% of incoming radiation power is directly deposited at the target surface. Then for $F(\lambda=10) \approx 20$ and $\zeta = 1$;

$$\frac{L}{R_{d0}} \approx 200\frac{U(m/s)}{W_0(MW/cm^2)}. \tag{10}$$

The vaporization energy of sublimation in the form of triatomic molecules: q_v (C_3) ≈ 40 kJ/cm^3, thus $\lambda(C_3) \approx 3.6$ and $W_s/W_0 \approx 0.22$. Then for F ($\lambda = 3.6$) = 6.63 and ζ=1;

$$\frac{L}{R_{d0}} \approx 67 \frac{U(m/s)}{W_0(MW/cm^2)}. \qquad (11)$$

The MP size from experiments at the MKT facility was shown to be $R_d \leq 10$ μm [16]. Because of the more radiative nature of carbon elements, the radiation power to the target surface during disruption is calculated to be less than that for a lithium target, i.e., $W_0 \leq 0.5$ MW/cm^2, thus L (C_1) ≈ 4000 R_{d0} and L ≈ 4 cm; and for L (C_3) ≈ 1300 R_{d0} gives L ≈ 1 cm. Greater MP flight distances are usually due to higher heat of vaporization.

It is also important to take into account that graphite grains with size less than 10 μm can easily be split into crystallites measuring a few hundreds of Angstroms. Therefore, it is expected for a graphite target that eroded dust can be vaporized at even shorter distances above the target surface.

In the above analysis, it was assumed that the MP are emitted normal to the target surface. It is important to consider that some MP are emitted near the target edge with bandwidth $\Delta y \leq L$ and therefore will not be fully vaporized. A fraction of MP mass ≈ $2L/L_d$, where L_d is target width, leaves the vapor cloud without being vaporized and is redeposited on nearby components. Nevertheless, total erosion mass loss can increase by the ratio ≈ $2L/L_d$ ($1+\lambda$). This could be particularly significant in disruption simulation experiments where the exposed target is of the order of MP vaporization length L and therefore the actual erosion is substantially over estimated in reactor conditions.

Vapor flow along the target surface due to hydrodynamic turbulence that is excited by modes of flute-type instability in an inclined and strong magnetic field can be important for two reasons. First, such flow can excite Kelvin-Helmholtz instability of capillary waves in the molten layer surface and can cause additional splashing and droplet formation during the nonlinear stage of these waves. Second, droplets blown

away because of vapor wind will have high velocity components along the vapor wind direction, i.e., along the plate surface. Such droplets will have a much shorter flight time in the hot vapor cloud and therefore will have no time to absorb the incoming radiation energy through droplet vaporization. Therefore, mass losses in this case can also be significant. The existence of such turbulence remains unclear up to now and requires further modeling and simulation experiments.

4. Total Mass Losses and Lifetime of PFMs

Numerical calculations have shown that there are several stages of plasma flow interaction with target materials. Initially, SOL particles interact directly with the target surface. Due to the high power load, the material surface is heated to a temperature sufficient for intense vaporization. A vapor cloud is quickly formed with enough mass to stop SOL particles and the vapor is heated to temperatures of a few tens of eV. Therefore, most deposited plasma power is radiated back by the shielding vapor layer. The shielding layer forms in time duration, τ_{vapor}, of ≈10-20 μs. Target surface temperature decreases due to reduction of radiation power at the surface, and only after some time, τ_{cond}, the surface temperature rises again and reaches a "vaporization temperature" sufficient to start volume-bubble boiling or brittle destruction. This vaporization temperature corresponds to the saturation temperature at the vapor-cloud pressure of a few tens of atm. Then, after time $\geq \tau_{delay} = \tau_{vapor} + \tau_{cond}$, the process has a quasistationary character in which the radiation power to the surface is spent for vaporization, droplet emission, and heat conduction into the target bulk.

The τ_{cond} depends on the incoming radiation power to the surface and material thermodynamic properties. It can be estimated by

$$\tau_{cond} \approx \frac{C_p \kappa T_v}{W_o^2}, \qquad (12)$$

where C_p is target specific heat, κ is target thermal conductivity, T_v is vaporization temperature, and W_o is power to the target surface. It can be seen from Eq. 12 that τ_{cond} is

linearly proportional to vaporization temperature; therefore, strong mass losses due to ablation of high-boiling materials starts only after a longer delay. The delay time τ_{delay} is calculated for the candidate materials Be, C, and W to be ≈ 70, 150, and 300 μs, respectively.

The time dependence of both melting and splashing fronts of a tungsten target for a net radiation power to the surface of 100 kW/cm^2 is shown in Fig. 3. The melting front moves initially with time as $t^{-1/2}$ for time $t < \tau_{delay}$. When splashing starts at temperature $T = T_v$, and liquid droplets are removed, the distance between the splashing surface and the melting front remains constant. This means that all incoming radiation power is spent for splashing.

Figure 4 shows the time dependence of tungsten splashing-erosion depth for various radiation power levels on a tungsten surface without droplet shielding effect. The time τ_{delay} required to heat the surface to a temperature above the splashing condition ($T > T_{vap}(P_v)$, where P_v is plasma pressure above the target surface) depends on incoming radiation power S_{rad} as S^{-2}. It can be seen that decreasing S_{rad} from 0.3 MW/cm^2 to 0.1 MW/cm^2 increases the delay time from 60 μs to 600 μs, respectively. This finding has two significant implications. First is that the level of radiation power substantially increases the MP erosion rate (from 100 μm at 0.1 MW/cm^2 to 900 μm at 0.3 MW/cm^2, without droplet shielding). Second, it can explain why in some simulation experiments that significant splashing, particularly with high-Z targets such as tungsten, was not seen because of the short time duration of these simulation devices which is less than the time delay required for S_{rad} associated with such experiments. Therefore, for adequate modeling and simulation of the effect of tokamak instability events on erosion lifetime, facilities with long time duration of more than 300 μs are needed. In the VIKA disruption simulation facility [17], it was shown that for different target materials, significant erosion starts after some delay time similar to that predicted by Eq. 12.

Therefore, mass losses of divertor plate and nearby components depend strongly on the dynamics and evolution of the vapor cloud and droplets or macroscopic particles.

The main concern is the time to start ablation and the existence of both vapor and droplet shielding. Mass losses and lifetime of PFMs due to vaporization and ablation depend strongly on interaction conditions dictating the existence or absence of both vapor cloud and droplet shields. The vapor shield exists if the vapor cloud is well confined by a strong magnetic field. For a divertor plate, the existence of vapor shielding depends on MHD instabilities in the vapor cloud, which can result in turbulent diffusion across the magnetic field. In an inclined magnetic field, turbulent diffusion results in vapor flow and loss ("the vapor wind") along the poloidal direction that decreases the efficiency of vapor shielding. Blowing away of droplets or MP by the vapor wind is more serious because decreasing the droplet shielding significantly enhances droplet emission. For nearby components of the divertor system, existence of shielding depends, in addition, on the geometrical locations relative to magnetic field structure.

There are four possible erosion scenarios during plasma/target interaction. Figure 5 compares the erosion depth of both Be and graphite targets for these cases with and without both vapor shielding and droplet shielding. In case 1, i.e., absence of both shielding mechanisms (no vapor shielding, i.e., vapor is not well confined and there is no droplet shielding, so that droplets are splashed away from the incoming plasma), all incoming power will be spent in splashing erosion of the liquid surface. Erosion loss is very high, and this case may represent a disruption simulation device in which the incident plasma has a very high dynamic pressure exceeding the magnetic field pressure that is capable of blowing off the initial vapor cloud and liquid layers. Case 1 may also resemble a tokamak condition in which a strong MHD vapor turbulence develops and result in fast removal of vapor and droplets along target surface. In case 2, without vapor shielding and splashing (or ablation), all incoming power will be spent in vaporizing the target surface. This may occur if the vapor cloud is removed for any reason and the target material does not melt or splash/destruct.

In case 3, with vapor shielding but without droplet shielding (droplets are removed from incoming power), the net incoming radiation power to target surface is spent in splashing. This situation can occur on nearby components during a disruption on

the divertor plate, in which the intense photon radiation from the hot vapor cloud deposits its power at locations with different orientations to the magnetic field lines; as a result, the vapor cloud is not well confined. This may also be true in many of the disruption simulation devices such as plasma guns and electron beams where the plasma or particle flow has a small cross section and MP do not have enough flight time in the vapor cloud to absorb the incoming radiation power and shield the target surface. This can also occur in tokamak conditions with moderate levels of turbulence in which the vapor wind is strong enough to blow away droplets but not strong enough to remove all vapor; thus, the remaining vapor cloud has enough depth to stop most incoming plasma particles and radiate back the deposited power. Ablation can increase mass losses of by $\approx$ 4-5 times. Therefore, droplet removal is critical because droplet shielding results in all radiation from the vapor cloud going to the target surface to be spent in vaporization, mostly through the intermediate process of droplet emission and further vaporization during droplet flight across the vapor cloud.

The fourth case is the most desirable and can be realized in a tokamak device if the vapor cloud is well confined with no MHD effects. Therefore, a well-confined vapor and droplet cloud can reduce erosion losses by up to two orders of magnitude. It should be noted that these results are valid at longer time $t > \tau_{delay}$, i.e., when the surface temperature achieves its quasistationary value in a stable vapor-plasma. For a shorter time duration, vaporization losses in the case of vapor and droplet shielding can be calculated directly. However, droplets and macroscopic particles that are ejected near target edges and/or having larger sizes or moving with higher velocities will not have sufficient time to completely vaporize and shield the target surface; therefore, erosion lifetime is lower. In addition, higher droplet velocities due to the drag force of the fast-expanding vapor, or due to the high explosive pressure in the brittle destruction mechanism, can increase mass loss because the droplets will spend less time in the hot vapor cloud.

The observed increase in the eroded area, which is larger than the footprint of the incident plasma flow in some simulation experiments, can be explained as the result of

vapor-radiation interaction with the target surface outside the plasma flow spot [2] or as the result of MHD instabilities in the vapor cloud [18]. In addition, slight shifting of the vapor cloud due to $[\vec{E}x\vec{B}]$ force may also occur along the target. However, these problems have not been well investigated and require more analysis and simulation.

To summarize the simulation results, overheating of the plate surface causes macroscopic particles and droplets to be ejected/splashed upstream and away from the surface. These particles then absorb some part of the incoming vapor radiation. The net fraction of radiation power reaching the divertor surface is determined mainly by the ratio of vaporization to splashing energies. The distance at which macroscopic particles or droplets are completely vaporized is about $L \leq 1$ cm. Therefore, the mixture of vapor and macroscopic particles exists only very near the divertor surface. Despite initial large splashing erosion, total erosion of the divertor plate is defined only by vaporization losses, including both divertor plate vaporization and MP vaporization. Again, this is true only if both the vapor cloud and the splashed droplets are well confined in front of the disrupting plasma. However, loss of vapor confinement can occur as a result of the MHD instability that arises due to distortion of the oblique magnetic field lines by the expanding vapor plasma [18]. In this case, the developed turbulence results in vapor flow along the divertor plate surface. Due to this flow, Kelvin-Helmholtz instability of unstable surface waves occurs, resulting in splashing. Second, this vapor flow blows both vapor and droplets along the target surface, reducing vapor-shielding efficiency because of vapor cloud removal. In addition, efficiency of droplet shielding is reduced due to decreased droplet exposure time in the depleted vapor.

Efficient vapor shielding that protects the divertor plates from high heat loads means that >90% of incoming power is radiated to nearby locations. Therefore, the problem of erosion of other parts in a closed divertor system becomes more serious. It was shown both experimentally [19] and theoretically [20] that interaction of this "secondary" radiation with other components results in the same consequences as the primary interaction of the SOL plasma, i.e., vapor cloud formation, splashing, etc. Moreover, it may be very difficult for such vapor clouds to be well confined, especially if

the magnetic field angle of inclination with different oriented surfaces is very low. Erosion of such nearby components could be estimated as done in case 1, because of the absence of both shielding effects.

Thermal-quench disruptions have no significant thermal effect on structural materials and coolant channels, due to the short deposition time. However, VDEs, in addition to causing severe surface melting and erosion, can result in substantial damage to these components [1]. One concern is the higher temperature observed in the structural material, particularly at the interface with the coating materials. Higher temperatures cause high thermal stresses in the structure and seriously degrade the integrity of the interface bonding, which may lead to detachment of the coating from the structural material. The copper-structure surface temperature during a VDE has been calculated with different tungsten, beryllium, or carbon tiles/coatings. With a tungsten coating, the copper surface interface can actually melt. Only beryllium coatings of reasonable thickness (<5-10 mm) or very thick carbon tiles (>20 mm) can withstand the acceptable temperature rise in the copper structure for the conditions shown. However, beryllium and carbon coating materials will suffer significant surface erosion while protecting the structural copper substrate. A thin free-surface layer (≈1-2 cm thick) of a liquid metal such as lithium would be an ideal solution to completely protect the structure and offer unlimited PFC erosion lifetime. The structural materials during the VDE will have no high-temperature effects because the liquid metal will remove the heat by either convection (moving film) or intense vaporization (stationary film). However, problems related to plasma/free-surface liquid-metal interactions during normal operations must be carefully examined.

5. Conclusions

Erosion of plasma-facing materials is governed by both the characteristics and distribution of incident plasma particles from the SOL, as well as by processes resulting in vapor and droplet formation and shielding. Models and theories have been developed for material erosion during intense deposition of energy on target surfaces. Most mass

losses resulting from plasma/target interaction during plasma instabilities are from ablation, i.e., emission of droplets due to liquid splashing or macroscopic particles as a result of brittle destruction. Therefore, a mixture of vapor cloud and macroscopic particles exists near the target surface. Influence of such "aerosol" on vapor cloud dynamics and the net heat load onto the target surface depends on the geometrical location of the divertor system and the existence of MHD turbulence of the vapor plasma in an oblique and strong magnetic fields. Various cases of existence or absence of vapor and droplet cloud shielding, as well as the existence of MHD instabilities, are considered and the corresponding mass losses are estimated, as are lifetimes of plasma-facing materials. The use of a renewable material such as free-surface liquid lithium may significantly extend the lifetime of PFMs and substantially enhance the tokamak concept for power-production reactors. In general, plasma instabilities must be avoided or sharply minimized. Moreover, the effects of redeposited debris from the eroded materials on plasma contamination and on subsequent reactor operations must be further studied.

Acknowledgment

This work is supported by the U.S. Department of Energy, Office of Fusion Energy, under Contract W-31-109-Eng-38.

6. References

[1] A. Hassanein and I. Konkashbaev, "Theory and Models of Material Erosion and Lifetime during Plasma Instabilities in a Tokamak Environment," presented at the 5th Int. Symp. on Fusion Technology (ISFNT-5), Sept. 19-24, 1999, Rome, Italy. To be published in Fusion Eng. & Design.

[2] A. Hassanein and I. Konkashbaev, J. Nucl. Mater., 273 (1999) 326.

[3] A. Hassanein, Fusion Technol. Vol. 30 (1996) 713.

[4] A. Hassanein and I. Konkashbaev, Suppl. J. Nucl. Fusion 5 (1994) 193.

[5] V. Belan et al., J. Nucl. Mater. 233-237 (1996) 763.

[6] V. Litunovsky et al., Fusion Technol., B. Beaumont, P. Libeyre, B. de Gentile, and G. Tonon, eds. (1998) 59.

[7] N. I. Arkhipov et al., J. Nucl. Mater. 233-237 (1996) 767.

[8] A. Hassanein, Fusion Technol. 15 (1989) 513.

[9] V. Litunovsky et al., 16th IEEE/NPSS Symp. on Fusion Engineering, Sept. 30-Oct. 5, Champaign, IL (1995) 435.

[10] T. Burtseva et al., Plasma Devices and Operations, Vol. 4 (1995) 31.

[11] J. Linke et al., Fusion Technol., B. Keen, M. Huguet, and R. Hemsworth, eds. (1991) 428.

[12] J. Van der laan, J. Nucl. Mater. 162-164 (1989) 964.

[13] A. V. Burdakov et al., J. Nucl. Mater. 233-237 (1996) 697.

[14] A. Hassanein and I. Konkashbaev, J. Nucl. Mater 233-237 (1996) 713.

[15] A. Hassanein et al., Fusion Technol., K. Herschbach, W. Maurer, and J. E. Vetter, eds. (1994) 223.

[16] M. Guseva et al., J. Technical Physics, 66, No. 6, (1996) 106 (in Russian).

[17] V. Litunovsky et al., Proc. 20th Symp. on Fusion Technology (SOFT), Sept. 7-11, Marseille, France, Vol. 1 (1998) 59.

[18] A. Hassanein and I. Konkashbaev, Plasma Devices and Operations, Vol. 5 (1998) 297.

[19] V. Safronov, N. Arkhipov, et al., Fusion Technol., B. Beaumont, P. Libeyre, B. de Gentile, and G. Tonon, eds., (1998) 105.

[20] A. Hassanein and I. Konkashbaev, Fusion Technol., C. Varandas and F. Serra, eds., (1996) 379.

Figure Captions

Figure 1 Time evolution of tungsten surface temperature, melt layer, and vaporization thickness during plasma instabilities.

Figure 2 Schematic illustration of droplet and macroscopic shielding concept during plasma/material interaction following plasma instabilities.

Figure 3 Time dependence of melting and splashing fronts due to radiation power to tungsten target.

Figure 4 Effect of net radiation power to target surface on tungsten total splashing thickness without droplet shielding.

Figure 5 Effect of vapor-cloud shielding and macroscopic particle/droplet shielding on total mass loss for Be and C during disruption.

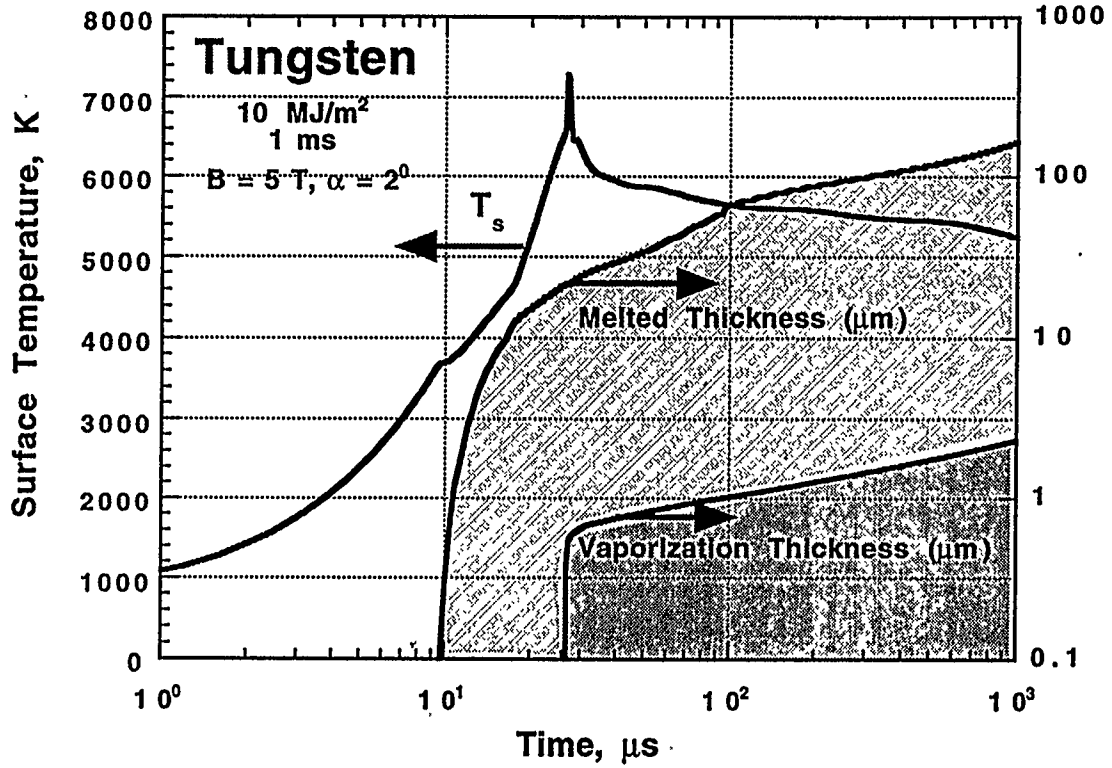
Tungsten
10 MJ/m²
1 ms
B = 5 T, α = 2⁰
T_s
Melted Thickness (μm)
Vaporization Thickness (μm)
Surface Temperature, K
Time, μs
8000
7000
6000
5000
4000
3000
2000
1000
0
1000
100
10
1
0.1
10⁰
10¹
10²
10³

Fig (1)

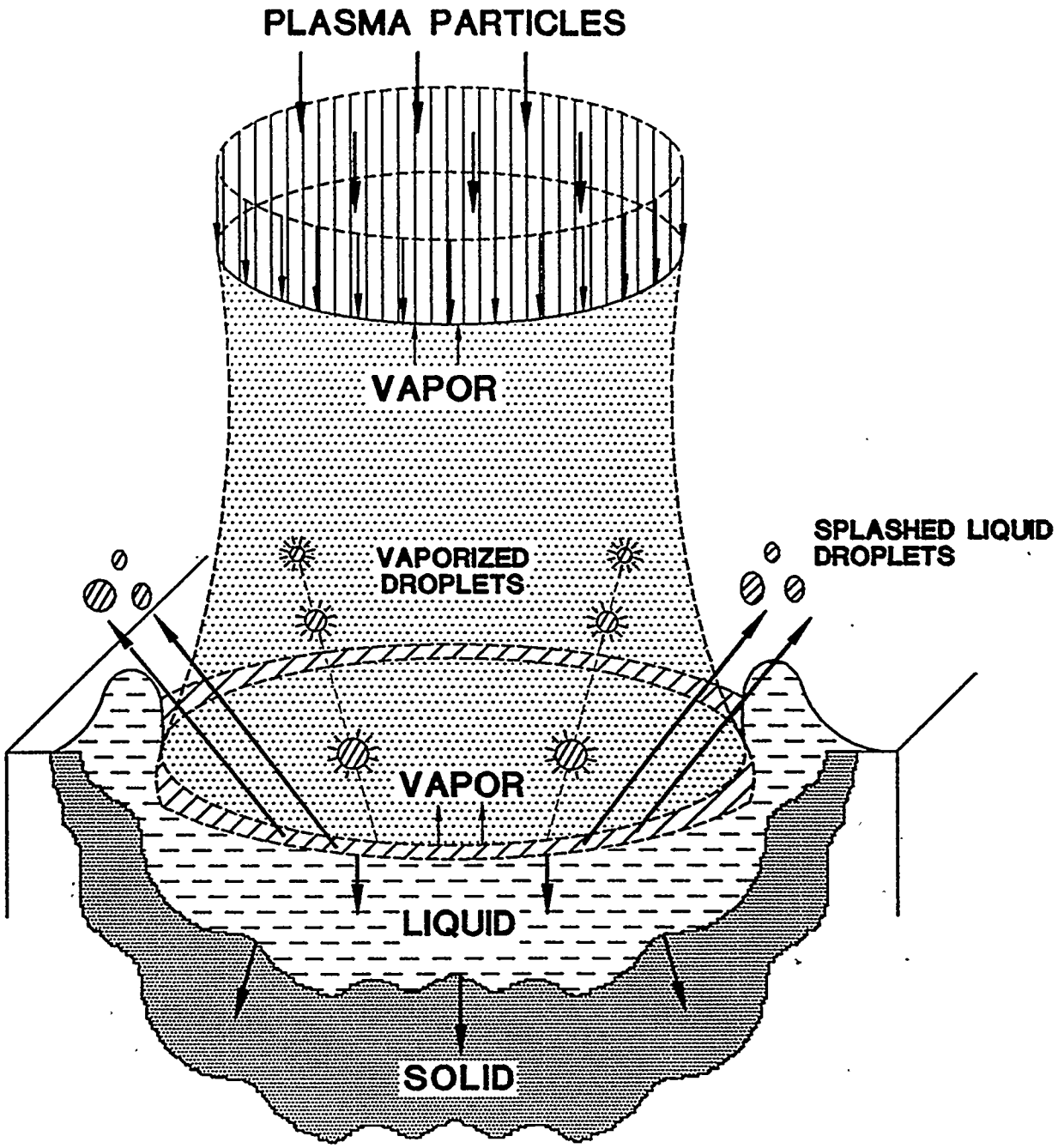
PLASMA PARTICLES
VAPOR
VAPORIZED DROPLETS
SPLASHED LIQUID DROPLETS
VAPOR
LIQUID
SOLID

Fig (2)

G10947

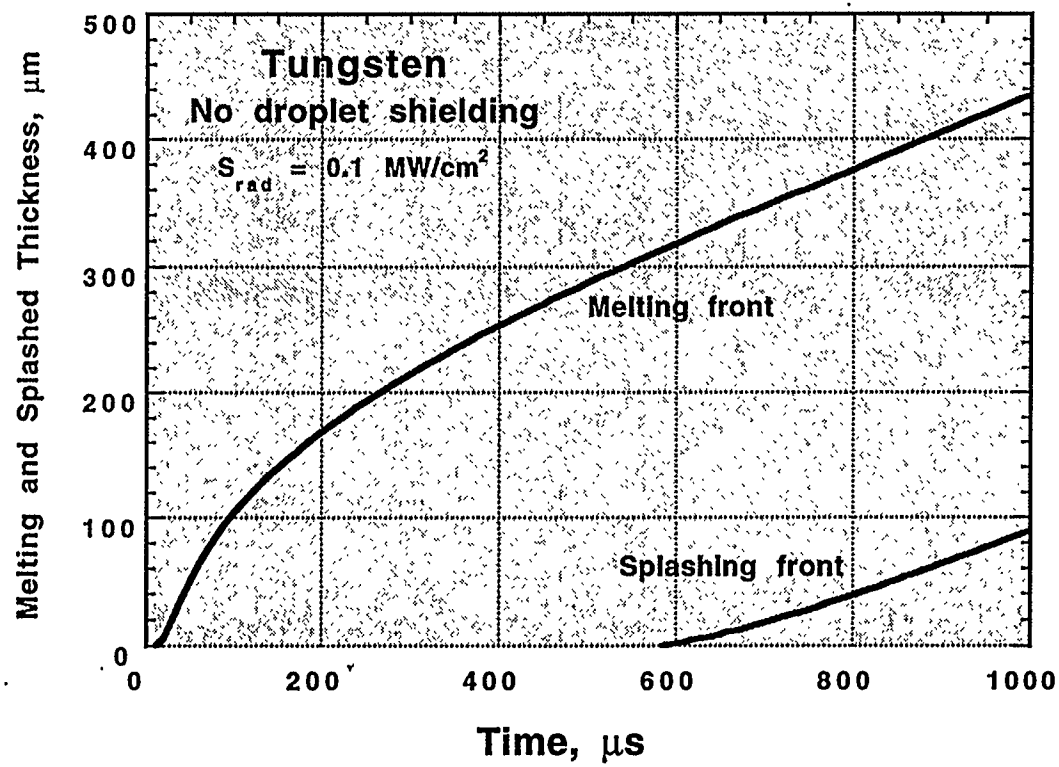
Tungsten
No droplet shielding
S rad = 0.1 MW/cm2
Melting front
Splashing front
Melting and Splashed Thickness, μm
Time, μs
0
100
200
300
400
500
0
200
400
600
800
1000

Fig (3)

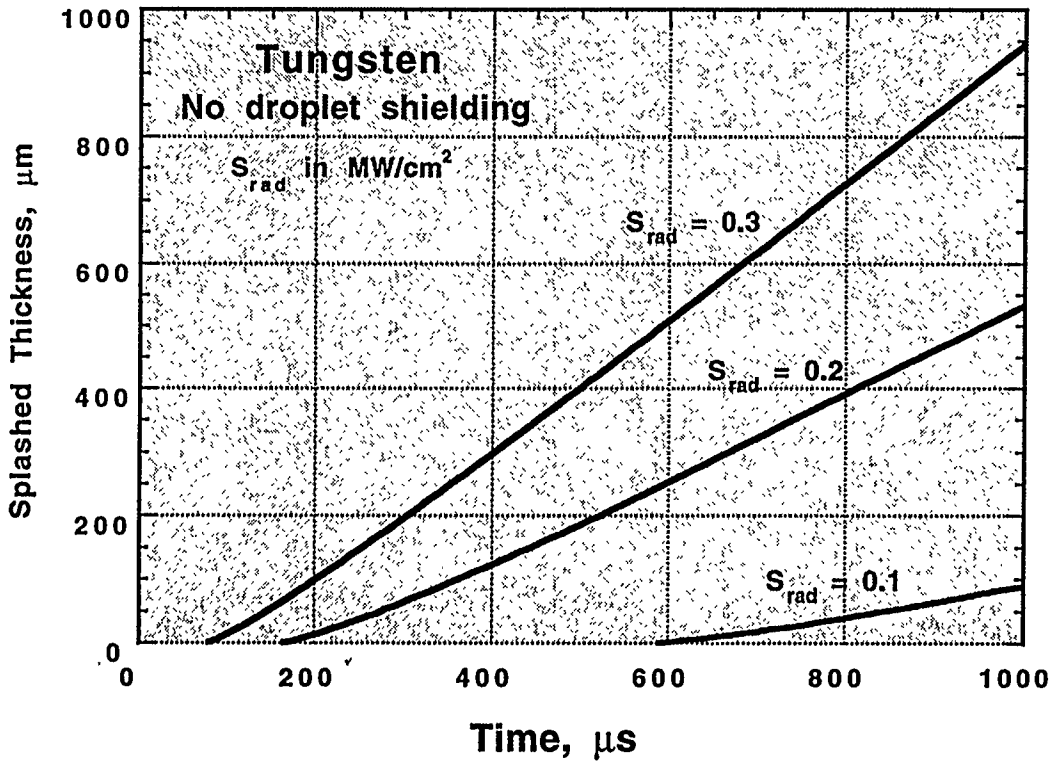
Tungsten
No droplet shielding
S rad in MW/cm2
S rad = 0.3
S rad = 0.2
S rad = 0.1
Splashed Thickness, µm
Time, µs
0
200
400
600
800
1000

Fig (4)